Fractonlike phases from subsystem symmetries

J. P. Ibieta-Jimenez,[*] L. N. Queiroz Xavier,[†] M. Petrucci,[‡] and P. Teotonio-Sobrinho[§]
Departamento de Física Matemática, Universidade de São Paulo, Rua do Matão Travessa R 187, CEP 05508-090, São Paulo, Brazil

(Received 8 November 2019; revised 15 June 2020; accepted 17 June 2020; published 2 July 2020)

We study models with fractonlike order based on $\mathbb{Z}_2$ lattice gauge theories with subsystem symmetries in two and three spatial dimensions. The three-dimensional (3D) model reduces to the 3D toric code when subsystem symmetry is broken, giving an example of a subsystem symmetry enriched topological phase. Although not topologically protected, its ground-state degeneracy has as leading contribution a term which grows exponentially with the square of the linear size of the system. Also, there are completely mobile gauge charges living along with immobile fractons. Our method shows that fractonlike phases are also present in more usual lattice gauge theories. We calculate the entanglement entropy S_A of these models in a subregion A of the lattice and show that it is equal to the logarithm of the ground-state degeneracy of a particular restriction of the full model to A.

DOI: 10.1103/PhysRevB.102.045104

I. INTRODUCTION

Since the discovery of the fractional quantum Hall (FQH) effect [1,2], it has been known that there are quantum phases of matter that cannot be explained by Landau's symmetry-breaking theory. Topologically ordered phases, of which FQH states are a standard example, encompass phases that are beyond the scope of Landau's theory. Intrinsic topological order can be characterized as exhibiting, among other properties, a ground-state degeneracy that depends on the topology of the underlying space in which the system lives [3] and long-range entangled ground states [4], which means that they cannot be transformed into product states by means of local unitary transformations. Another important feature of topological phases is the presence of anyonic excitations, which is essential to the potential application of topological order in fault-tolerant quantum computation [5,6]. A classical example of intrinsic topological order is Kitaev's toric code (TC) [5], first introduced in the context of quantum computation as a quantum error correction code and as a way of implementing a quantum memory. This model can be interpreted as a $\mathbb{Z}_2$ lattice gauge theory, and it is a particular case of a larger class of models known as quantum double models (QDMs) [5,7–9], which are topologically ordered exactly solvable models based on lattice gauge theories with arbitrary finite gauge groups.

It is also possible to have topological order with short-range entanglement of the ground states if there are global symmetries in the system. Phases with such behavior are known as symmetry-protected topological (SPT) phases, and they are characterized by the fact that entangled ground states cannot be transformed into nonentangled ones by means of local unitary transformations without breaking a global symmetry. The classification of SPT phases is known to be related to the group cohomology of the global symmetry group [10,11].

Global symmetries may also coexist with topological order. A topologically ordered system which respects a global symmetry may host anyons which carry fractionalized quantum numbers under this symmetry, a phenomenon known as symmetry fractionalization. For example, global $U(1)$ charge conservation in the fractional quantum Hall effect imposes a fractionalization of the electric charge of some of its quasiparticles [2]. The effect of global symmetries on topologically ordered states leads to the notion of symmetry-enriched topological phases. A system is in a symmetry-enriched topological phase if, by breaking the symmetry, the system still presents topological order [12–15].

Intrinsic topological order has its low-energy behavior described by topological quantum field theories, which are intimately connected to category theory [16]. In particular, string-net models [17], a more general framework that captures essential features of topological phases in two spatial dimensions, are obtained from fusion categories. It is becoming clear that, for systems in more than two dimensions, higher category theory and higher gauge theory [18,19] are essential to understand topological order. A variety of models of topological phases obtained from these structures can be found in the literature [20–22].

Recently, it was theorized that a new type of quantum phase of matter lies beyond the topological order framework. The so-called fracton order [23–25] refers to quantum phases of matter in which distinct ground states cannot be distinguished by local measurements, a feature shared with topologically ordered systems. However, the ground-state degeneracy exhibits a subextensive dependence on the system size, in contrast with the constant ground-state degeneracy of topologically ordered models. Also, the spectrum of fracton models is composed by quasiparticles with several mobility restrictions, and some of the excitations, the so-called fractons, are completely

[*]pibieta@if.usp.br
[†]lucasnix@if.usp.br
[‡]marzia@if.usp.br
[§]teotonio@if.usp.br

immobile, i.e., they cannot be moved by stringlike operators, in contrast with anyons in topologically ordered models which are free to move around the lattice.

Based on the mobility of its excitations, it is common to divide gapped fracton phases into two distinct types. In type-I fracton phases, immobile fractons appear at the corners of membranelike operators, and there are other quasiparticles that can move along subdimensional manifolds, for example, along lines or planes if the system is three dimensional (3D). In type-II fracton phases, the only excitations are completely immobile fractons and they live at the corners of fractal-like operators. A more detailed description of the different types of fracton phases is presented in [26]. Standard examples of models exhibiting type-I and type-II fracton phases are the X-cube model [24,27] and the Haah code [28], respectively. Both are exactly solvable spin models in three dimensions. Gapped fracton models are related to glassy physics and localization [23,29–33] and they present potential applications to quantum information [28,34–40]. There are also gapless fracton models arising from the study of symmetric tensor gauge theories [41–46]. This approach allows a connection of fracton models with elasticity theory and gravity [47–49], and some gapped fracton phases can be obtained from symmetric tensor gauge theories defined on a lattice by a Higgs mechanism [44,50]. The relation between gapless fracton phases and gravity suggests that fractonlike models may be considered as toy models for the holographic principle [51,52].

There are ways of generating fracton phases from known topologically ordered models. For example, the X-cube model can be obtained by coupling layers of two-dimensional (2D) toric codes [45,53,54]. However, the most common manner in which fracton models are obtained is by considering lattice spin systems with subsystem symmetries as generalized Abelian lattice gauge theories [24]. Fracton phases are then constructed through a process of gauging the subsystem symmetries [55,56]. Another method to obtain new fracton phases is by twisting the usual fracton models [57] and by enriching $U(1)$ gauge theories with a global symmetry [58].

In this paper, we study some models with fractonlike order based on lattice gauge theories with subsystem symmetries in two and three spatial dimensions. By fractonlike order we mean that the excited states of the models considered here are confined to certain regions of the lattice, i.e., they cannot move without some energy cost, and thus they are immobile fractons. However, although the ground-state degeneracy of our models exhibits a dependence on the geometry of the lattice, as is the case in most of the standard fracton models, it is not stable under the action of local perturbations, i.e., it is not topologically protected. The two-dimensional model we present here is similar to the one introduced in [51,52], and serves as a guide to the study of the three-dimensional model. This model reduces to the 3D toric code when the system is perturbed by operators that break the subsystem symmetry, realizing an example of a subsystem symmetry-enriched topological phase. The ground-state degeneracy of this model grows exponentially with the square of the linear size of the system, and there is also a topological contribution to the ground-state degeneracy when the system is defined on topologically nontrivial manifolds. Moreover, while this model has completely immobile fractons as some of its excitations, there are also quasiparticles in the spectrum that are fully mobile. Even though some known models also present ground-state degeneracy that grows exponentially with the square of the linear size of the system [59] and mobile charges [60,61], the method introduced here gives an alternative construction of fractonlike models that differs from the usual ones. We calculate the entanglement entropy S_A in a subregion A of these models and show that $S_A = \log(\mathrm{GSD}_{\tilde{A}})$, where $\mathrm{GSD}_{\tilde{A}}$ is the ground-state degeneracy of a particular restriction of the full model to the subregion A, a result in agreement with [62].

The outline of this paper is the following. In Sec. II, we review a two-dimensional fractonlike model and describe its properties, explaining how its subsystem symmetries are related to its fractonlike properties. In Sec. III, we introduce a three-dimensional fractonlike model and analyze its fracton properties, borrowing some ideas from Sec. II. In Sec. IV, we calculate the entanglement entropy S_A, in a subregion A, of the models studied in the previous sections, and show that they obey the relation $S_A = \log(\mathrm{GSD}_{\tilde{A}})$, where the meaning of $\tilde{A}$ will be clarified. In Sec. V, we make some remarks about how one could study models of fractonlike phases based on gauge theories with arbitrary finite gauge groups.

II. REVIEW OF FRACTONLIKE ORDER IN TWO DIMENSIONS

In this section, we start by reviewing a simple example of a model exhibiting fractonlike order in two spatial dimensions. This 2D model was first introduced in [63,64] to describe a superconducting state and it is known as the Xu-Moore model or *plaquette Ising model*. The model is shown to have one-dimensional subsystem symmetry in [55,65] and thus considered as a model for fractonlike order in [51,52], as we will review. Its classical version is known as the *gonihedric Ising model*, a particular case of the eight-vertex model [52,66], studied in the context of string theory and spin-glass physics in [67–70] and references therein.

A. The model

Consider the discretization of a two-dimensional oriented manifold M. For simplicity, we take the discretization to be described by a square lattice K. The lattice is composed by a set of vertices K_0, a set of links K_1, and a set of plaquettes K_2. To each vertex $v \in K_0$ we associate a local Hilbert space $\mathcal{H}_v$ with basis $\{|1\rangle, |-1\rangle\}$. In other words, a spin-1/2 degree of freedom sits at each vertex v. Consequently, the total Hilbert space of the model, $\mathcal{H}$, is given by the tensor product of the local Hilbert spaces over all vertices:

$$\mathcal{H} := \bigotimes_v \mathcal{H}_v. \tag{1}$$

For each plaquette $p \in K_2$, we define the operator

$$B_p = \frac{1}{2}\left(\bigotimes_{v\in p} \mathbb{1}_v + \bigotimes_{v\in p} \sigma_v^z\right), \tag{2}$$

that acts over the spins at the four vertices of p. This operator collects the values of spins at the vertices of p, such that it favors configurations with even number of $|-1\rangle$ around plaquettes. Although this operator seems to be just comparing

the degrees of freedom at the vertices around plaquettes, a more physical interpretation of its action will be given in Sec. V. The global $\mathbb{Z}_2$ symmetry of the model is made part of the Hamiltonian by means of the projector

$$A = \frac{1}{2}\left(\bigotimes_{v\in K_0} \mathbb{1}_v + \bigotimes_{v\in K_0} \sigma_v^x\right), \tag{3}$$

where the tensor product is taken over all vertices in K_0. This operator enforces a global gauge transformation on the system. Given (2) and (3), the Hamiltonian is defined by

$$H = -A - \sum_p B_p. \tag{4}$$

The global $\mathbb{Z}_2$ operator X given by

$$X = \bigotimes_{v\in K_0} \sigma_v^x \tag{5}$$

commutes with H.

B. Fracton properties

There seems to be three essential features that characterize fracton phases of matter: the subextensive behavior of the ground-state degeneracy, the fact that ground states are topologically protected, and the mobility constraints of the quasiparticles that belong to the spectrum of the model. The quasiparticles that are usually called fractons are completely immobile if considered individually. Bound states of fractons, however, can have increased mobility. Here we show that the model defined in Sec. II A indeed supports quasiparticles with restricted mobility and a ground-state degeneracy that grows exponentially with the system's size. However, this degeneracy can be lifted by local stabilizer operators and thus its ground states are not topologically protected. Hence, when perturbations to the system do not break the subsystem symmetry, we consider this model as an example of fractonlike order.

1. Ground-state degeneracy

Since the operators A and B_p commute for every plaquette p, we can solve this Hamiltonian exactly. Moreover, the operators A and B_p are projectors, so their spectrum is known. This allows us to characterize the ground-state subspace of the model as

$$\mathcal{H}_0 = \{|\psi\rangle \in \mathcal{H} \,|\, A\,|\psi\rangle = |\psi\rangle \text{ and } B_p\,|\psi\rangle = |\psi\rangle\},$$

for every plaquette $p \in K_2$. Let us now construct such states. To start, let $|+\rangle \in \mathcal{H}$ be the state where every vertex spin in the lattice is in the $|+1\rangle_v$ configuration, namely,

$$|+\rangle = \bigotimes_v |+1\rangle_v .$$

Similarly, the state where all local degrees of freedom are in the $|-1\rangle_v$ state is written

$$|-\rangle = \bigotimes_v |-1\rangle_v .$$

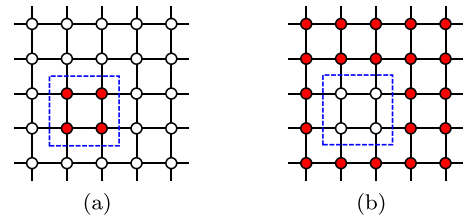

FIG. 1. The domain wall (in blue) of (a) separates two regions with different spin configurations. The same domain wall also determines the separation between configurations of (b). More importantly, the configuration in (a) is gauge equivalent to that of (b).

It is not difficult to see that the two states above satisfy the condition $B_p\,|\psi\rangle = |\psi\rangle$ for all plaquettes $p \in K_2$. Then, the state $|\psi_0\rangle = A\,|+\rangle = A\,|-\rangle = \frac{1}{2}(|+\rangle + |-\rangle)$ is a ground state.

Now, in order to construct other ground states, we will introduce a graphical notation to represent the basis states of $\mathcal{H}$ as follows: one can color (red) any vertex that holds a $|-1\rangle_v$ local degree of freedom (see Fig. 1). Furthermore, domain walls separating two regions with different spin configuration can be drawn. In general, a single domain wall is associated with two basis states of $\mathcal{H}$, as shown in Fig. 1. However, because of the global gauge transformation the two basis states associated to one domain-wall diagram are gauge equivalent. This means that domain walls are enough to represent gauge equivalence classes of basis states, or *physical states*. For example, in Fig. 2 we show two domain-wall diagrams and the respective states they represent.

The trivial ground state, $|\psi_0\rangle$, is represented by a diagram with no domain walls, as shown in Fig. 2(a). On the other hand, the diagram at the left of Fig. 2(b) stands for a state resulting from a linear combination of states with the given domain-wall configuration; this state is actually an elementary excited state of the model as we will see in Sec. II B 2.

Other ground states are given by gauge-equivalence classes of states in $\mathcal{H}$ on which B_p acts trivially (i.e., as an identity operator), for every $p \in K_2$. This means that every state obtained by applying the global gauge transformation on a trivial eigenstate of B_p, for all p, is a ground state. In order to be

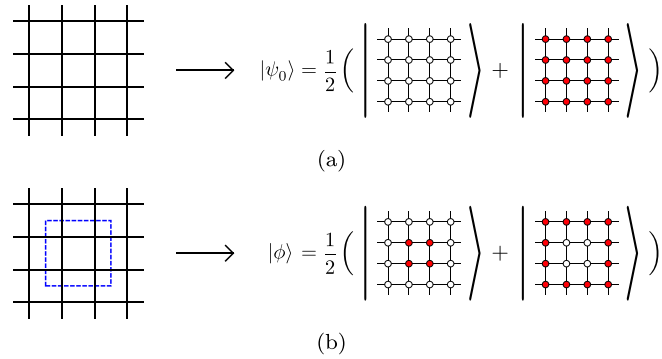

FIG. 2. In (a) the domain-wall diagram at the left represents the linear combinations of states at the right, in this case the ground state $|\psi_0\rangle = A\,|+\rangle$. In (b) the diagram at the left represents the state $|\phi\rangle$, which in fact is an excited state of the model.

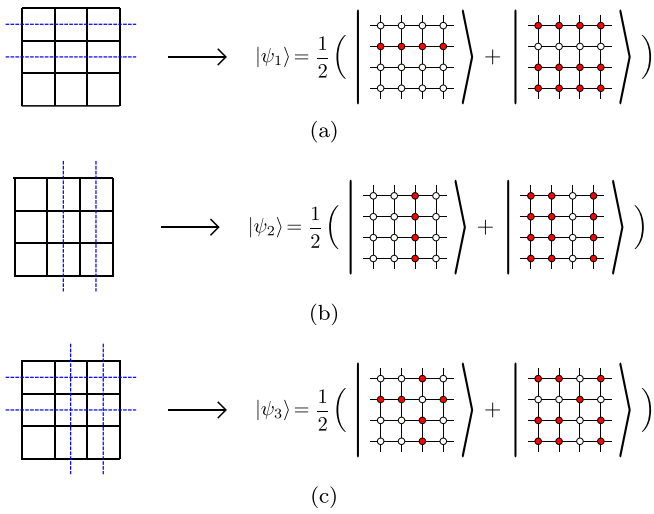

FIG. 3. Some possible ground states of the model. The domain-wall lines must begin and end at the boundary of the lattice.

invariant under B_p, a state must have either an even number of vertices with $|-1\rangle_v$ spins at each plaquette of the lattice or no $|-1\rangle_v$ spins at all. The latter case is taken care of by the state $|\psi_0\rangle$. Examples of the former case are illustrated in Fig. 3. The domain-wall lines must begin and end at the boundary of M. In case M has no boundary, the starting points of the blue domain-wall lines must be identified with its ending points. Essentially, domain-wall lines cannot have corners, i.e., every domain-wall line that enters a plaquette must exit it in the diametrically opposite side, as opposed to Fig. 2(b), which clearly represents an excited state because it has plaquettes with an odd number of vertices with spin $|-1\rangle$. Since the global gauge transformation A does not change domain-wall diagrams, any domain-wall configuration that represents a (gauge equivalent) linear combination of trivial eigenstates of B_p, for every p, is a ground state.

Note that we can have ground states with an arbitrary number of domain-wall lines in both directions. If M is a manifold with boundary and has dimension $L_x \times L_y$, this means that we can construct 2^{L_x} states with domain-wall lines in the x direction and 2^{L_y} states with domain-wall lines in the y direction, giving a total of

$$\mathrm{GSD} = 2^{L_x+L_y} \tag{6}$$

possible ground states. This shows the subextensive behavior of the ground-state degeneracy, which is characteristic of fracton models.

Nevertheless, there are local operators that commute with A and B_p, for every $p \in K_2$, that can be added to the Hamiltonian (4) which may destroy this degeneracy. As we will see in more detail in Sec. V A, we can define, for every link $l \in K_1$ in the lattice, the zero-holonomy operator [22,62]:

$$B_l = \frac{1}{2}\left(\bigotimes_{v\in\partial l} \mathbb{1}_v + \bigotimes_{v\in\partial l} \sigma_v^z \right). \tag{7}$$

For each plaquette $p \in K_2$, B_p can be regarded as an operator that compares the zero holonomy of parallel links that belong to the boundary ∂p of p. By this we mean that B_p gives an eigenvalue equal to one whenever parallel links in p have the same value of zero holonomy, and zero otherwise. Fix a plaquette $p' \in K_2$ and subtract from the Hamiltonian (4) a zero-holonomy operator $B_{l'}$, where l' is any link in the boundary $\partial p'$ of p'. The Hamiltonian is given by

$$H' = -A - \sum_{p\neq p'} B_p - B_{p'} - B_{l'}. \tag{8}$$

The ground states of H' must have a zero-holonomy value of 1 for the link l', which means that the spins at the vertices in the boundary of l' must be aligned. This introduces an additional constraint to the number of possible ground-state configurations of the plaquette p', and thus it reduces the ground-state degeneracy. Now, if we subtract two zero-holonomy operators, B_{l_1} and B_{l_2}, for two arbitrary links l_1 and l_2 in the boundary $\partial p'$ of p', this gives the following Hamiltonian:

$$H'' = -A - \sum_{p\neq p'} B_p - B_{p'} - B_{l_1} - B_{l_2}, \tag{9}$$

for $l_1, l_2 \in \partial p'$. The ground state of the system now must have a zero-holonomy value equal to 1 for both links l_1 and l_2 in $\partial p'$. This means that the spins at the vertices of each link in question must be aligned. If l_1 and l_2 are parallel to each other, this implies that the configuration of the plaquette p' is fixed; it either has all spins up or all spins down, and both are related by the global gauge transformation A, i.e., they represent the same physical state. An identical situation happens if l_1 and l_2 are perpendicular to each other. Therefore, adding zero-holonomy operators for the plaquette p' fixes its state, reducing the number of possible ground states. One can immediately see that, if we were to do the same process for every plaquette in the lattice, the degeneracy would be destroyed. Thus, we can decrease the ground-state degeneracy shown in Eq. (6) by adding local zero-holonomy operators, and therefore the ground states are not topologically protected. We can move from one state in the ground-state subspace to another by applying combinations of zero-holonomy operators.

This discussion can be summarized by noting that the model has subsystem symmetries given by operators that flip all spins along a straight line in the lattice. The ground-state degeneracy (6) can be calculated by counting the number of such operators, and the zero-holonomy operators explicitly break this subsystem symmetry, thus drastically reducing the number of ground states. It follows that, when the subsystem symmetry is respected, i.e., when perturbations do not break this symmetry, the model presents fractonlike order.

2. *Fracton excitations*

The excited states of the model $|\phi\rangle \in \mathcal{H}$ are states for which either $A|\phi\rangle = 0$ or, for some plaquette $p \in K_2$, $B_p|\phi\rangle = 0$. The excited state coming from the condition on the A operator is usually called *charge*. It is created by acting locally with σ^z on a single (arbitrary) vertex over a ground state of the model. The global nature of the gauge transformation makes it impossible to localize the charge, since we can only know whether a charge is present or not. For this reason, the charge is said to be global.

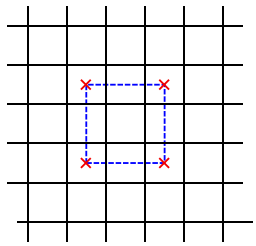

FIG. 4. The configuration of Fig. 2(b) has four fractons, represented here as four red crosses.

Plaquette excitations live at plaquettes that have a spin configuration with an odd number of vertices with spin $|-1\rangle_v$. Therefore, they live at the corners of domain walls. For example, the configuration in Fig. 2(b) has four excitations living at the four corners of the domain wall, as explicitly shown in Fig. 4. We can move pairs of excitations along straight lines, but individual excitations cannot be moved without costing energy to the system, and so they are essentially immobile. Therefore, plaquette excitations in this model are completely immobile fractons, and indeed the system described by the Hamiltonian in Eq. (4) exhibits fractonlike order in two dimensions. The arguments made for the calculation of the fracton properties of this model will be important to the study of other models we will define in the following sections.

III. FRACTONLIKE ORDER IN THREE DIMENSIONS

Here we introduce a model of fractonlike order in three spatial dimensions which reduces to the 3D toric code when subsystem symmetry is broken. This model exhibits some uncommon features, usually not present in the standard examples of fracton phases found in the literature. It is based on a $\mathbb{Z}_2$ lattice gauge theory with slightly modified holonomy operators, as we show in the following subsection.

A. The model

Let us consider a three-dimensional manifold M discretized by a regular cubic lattice. At each link l, we have a spin-1/2 degree of freedom, and the total Hilbert space of the model, which we call $\mathcal{H}$, is a product of all Hilbert spaces that sit at every link of the lattice. For each vertex v, we define the local gauge transformation which acts over spins at each link that shares the vertex v as follows:

$$A_v \left| \right\rangle = \frac{1}{2}\left(\left| \right\rangle + \left| \right\rangle \right), \tag{10}$$

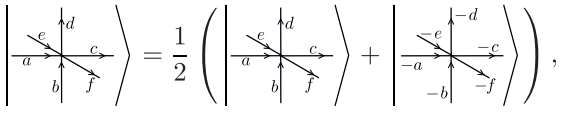

where $a, b, c, d, e, f \in \{1, -1\}$.

Next, for each elementary cube c, we define three holonomy operators, $B_c^{(x)}$, $B_c^{(y)}$, and $B_c^{(z)}$. To write them in a neat way, we represent the action of σ^z operators by coloring links, that is, links in blue are the ones over which a σ^z operator acts:

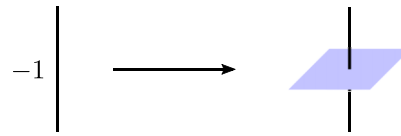

FIG. 5. Links holding a $|-1\rangle_l$ spin are represented by being crossed by a blue dual surface.

$$B_c^{(x)} \left| \right\rangle = \frac{1}{2}\left(\left| \right\rangle + \left| \right\rangle \right), \tag{11}$$

$$B_c^{(y)} \left| \right\rangle = \frac{1}{2}\left(\left| \right\rangle + \left| \right\rangle \right), \tag{12}$$

$$B_c^{(z)} \left| \right\rangle = \frac{1}{2}\left(\left| \right\rangle + \left| \right\rangle \right). \tag{13}$$

The operator $B_c^{(\mu)}$, for each direction $\mu = x, y, z$, checks if the holonomies of two opposite plaquettes in the direction μ are equal. This is obtained by taking the product of holonomies of the two plaquettes in the boundary of c the surfaces of which are orthogonal to μ. If both plaquettes have the same holonomy, this product is equal to $+1$ and we have an eigenstate of $B_c^{(\mu)}$ with eigenvalue $+1$. Likewise, if the two opposing plaquettes have different holonomies, the product is equal to -1 and we have an eigenstate of $B_c^{(\mu)}$ with zero eigenvalue, an excited state. We will say that a state has trivial holonomy in the direction μ if it is invariant under $B_c^{(\mu)}$, for every cube c in the lattice. The Hamiltonian is then given by

$$H = -\sum_v A_v - \sum_c \left(B_c^{(x)} + B_c^{(y)} + B_c^{(z)} \right). \tag{14}$$

B. Fracton properties

1. Ground-state degeneracy

As in the 2D model, the operators A_v and $B_c^{(\mu)}$ commute for all vertices v, cubes c, and directions μ in the lattice, so they can be diagonalized simultaneously. Also, the operators defined in Eqs. (10)–(13) are all projectors. This implies that the ground state of the model is given by all gauge-equivalence classes of states with trivial holonomy in all directions. Therefore, we must search for states such that, at each cube of the lattice, opposite plaquettes at each direction have the same holonomy. A natural ground state is $|\psi_0\rangle = \prod_v A_v |+\rangle$, where $|+\rangle \in \mathcal{H}$ is the state of the system where every link is in the $|+1\rangle_l$ state. To visualize these states, we introduce a graphical notation as follows: whenever a link has spin $|-1\rangle_l$, we draw a blue dual plaquette, as shown in Fig. 5, while links with spin $|+1\rangle_l$ have no additional drawings.

In this graphical notation, the action of A_v, for some vertex v, over the state $|+\rangle$ is understood as introducing a blue closed

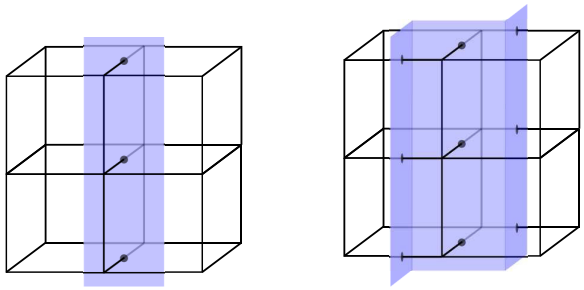

(a) (b)

FIG. 6. We show two possible ground-state configurations of the Hamiltonian in (14). The membrane must begin at the boundary of M and end at the diametrically opposite region. This means that, inside M, the membrane cannot curve to perpendicular directions.

surface around the vertex v. That is,

$$A_v \left| \right\rangle = \frac{1}{2} \left(\left| \right\rangle + \left| \right\rangle \right), \tag{15}$$

where the vertex v is the one at the center of the cubic lattice. Therefore, the state $|\psi_0\rangle$ is the superposition of all closed surfaces one can draw around vertices in the lattice and this ground state, as shown in Eq. (16), can be interpreted as a membrane gas much like the loop gas ground state of the toric code.

$$|\psi_0\rangle = N \left(\left| \right\rangle + \left| \right\rangle + \left| \right\rangle + \left| \right\rangle + \cdots \right), \tag{16}$$

We can have arbitrary compositions of such membrane configurations in every direction. Since the boundary lines of the membranes are gauge invariant, we use them to count how many possible ground-state configurations we can construct in this model. Therefore, the problem of counting ground states reduces to the problem of counting how many straight lines, beginning at one side of the boundary of M and ending at the diametrically opposite side, can be drawn on the manifold. We represent as a dot in the boundary of the manifold the beginning of a line that extends, in a straight fashion, through the interior of M to the diametrically opposite boundary point, as in Fig. 7. Each plaquette in the boundary of M either has a dot on it or it does not. For each boundary plane of M, there can be 2^{N_p} configurations of plaquettes with dots, where N_p is the number of plaquettes on the plane in question. Since M has dimensions $L_x \times L_y \times L_z$, the number of plaquettes in the boundary plane with dimensions $L_i \times L_j$ is $L_i L_j$, where $i, j = x, y, z$ and $i \neq j$. Thus, there are

$$\mathrm{GSD} = 2^{L_x L_y + L_x L_z + L_y L_z} \tag{17}$$

In the case that the manifold M has the topology of a three-torus, noncontractible closed surfaces give different equivalence classes of ground states. This increases the GSD with topological terms coming from the 3D toric code. In other words, the ground states of the 3D toric code are also ground states of our model, and there is a purely topological contribution to the ground state of the Hamiltonian (14). However, we are more interested in the contribution to the ground state of H that grows exponentially with the system size, the *subextensive terms*. For this reason we consider M as having the topology of a three-dimensional ball with dimensions $L_x \times L_y \times L_z$. States represented by membranes beginning at one of the boundaries of M and ending at the diametrically opposite boundary are also ground states of the model. For instance, the state represented by Fig. 6(a). Membranes can have arbitrary shapes in every one of the three directions as long as they end at the boundaries of M, as in Fig. 6(b). If the membranes do not end at the boundaries of M, we have an excited state, as in Fig. 9(a), where we have a link with spin $|-1\rangle$ shared by four cubes, which yields an excited state of cube operators in the z and y directions. In the interior of M, membranes cannot bend to perpendicular directions, for if they do we get excitations of cube operators at the folding regions of the bent membranes, as in Fig. 9(b) where the membrane of Fig. 9(a) is folded into the x direction, giving rise to excitations of $B_c^{(x)}$ operators at the folding line. The gauge transformation acts at vertices and can be pictured as adding a closed (dual) surface around the vertex at which it acts [see Eq. (15)]. Thus, gauge transformations can only deform membranes without changing their boundary:

possible ground states. It is useful to think of the ground states of this model as condensations of the 3D toric code model. Note that every ground state of the 3D toric code is a ground state of our model. Moreover, some excited states of the 3D toric code are ground states of our model. In particular, the

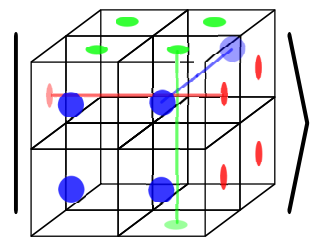

FIG. 7. To count the number of ground states of the Hamiltonian (14), we draw straight lines in the interior of M ending at dots on its boundary ∂M. These straight lines are boundary lines of the membranes representing ground states (see Fig. 6). The problem then reduces to counting how many dots we can draw on the boundary of M.

flux excitations of the TC that lie on a single plane are ground states of our model as well.

However, as happened to the 2D model of Sec. II, here there are local operators that commute with the Hamiltonian (14), i.e., local symmetry operators, which can lift the degeneracy given by Eq. (17) to that of the 3D toric code. To see this, fix a cube c' in the lattice and subtract from the Hamiltonian (14) a 3D toric code plaquette operator $B_{p'}$, where p' is some arbitrary plaquette in the boundary $\partial c'$ of c'. We have the Hamiltonian

$$H' = -\sum_{v} A_v - \sum_{c,\mu} B_c^{(\mu)} - B_{p'}, \tag{18}$$

where $\mu = x, y, z$. Ground states of H' must have a one-holonomy value of 1 for the plaquette p'. Since the cube operators $B_c^{(\mu)}$ constrain parallel plaquettes to have the same one-holonomy in the ground state, the plaquette which is parallel to p' will also have a one-holonomy value of 1. This reduces the number of ground-state configurations the cube c' can have, thus reducing the ground-state degeneracy. Now, if we subtract from the Hamiltonian (14) 3D toric code plaquette operators $B_{p'}$ for four of the six plaquettes in the boundary $\partial c'$ of c', the Hamiltonian is then given by

$$H'' = -\sum_{v} A_v - \sum_{c,\mu} B_c^{(\mu)} - \sum_{p' \in \partial c'} B_{p'}, \tag{19}$$

where $\mu = x, y, z$ and $B_{p'}$ are the one-holonomy operators of the 3D toric code for four specific plaquettes $p' \in \partial c'$. Now, the ground state of the model must have the four chosen plaquettes with holonomy equal to 1. This fixes the allowed ground-state configurations of the whole cube c', reducing further the number of allowed ground states. Subtracting 3D TC plaquette operators for every plaquette in the lattice, the ground-state degeneracy would end up being that of the 3D TC, because the contribution given by Eq. (17) would be destroyed and only the topological terms would survive. So, this model is not stable under local perturbations, reducing to the 3D toric code when local operators are added, and therefore it gives an example of a subsystem symmetry enriched topological phase, showing that not only topological phases enriched by global symmetries host fractonic behavior [58], but also subsystem symmetry-enriched ones. The question of whether the model presented here can be protected by a global symmetry is an open one.

We saw that we can go from the fractonlike model defined by Eq. (14) to the toric code by adding plaquette operators that break the subsystem symmetry. A reasonable question is then whether there is a way to go from the 3D toric code to the fractonlike model. To answer it, suppose we start with the 3D toric code defined on the three-torus, the Hamiltonian of which is

$$H_{\mathrm{TC}} = -\sum_{v} A_v - \sum_{p} B_p.$$

In the graphical notation introduced in this section, ground states of the toric code are represented by closed dual surfaces. Dual surfaces with boundary correspond to plaquette excitations. Consider an excited state of the toric code represented by a noncontractible dual ribbon, as in Fig. 8(a). In this figure, there are flux quasiparticles at all plaquettes along the

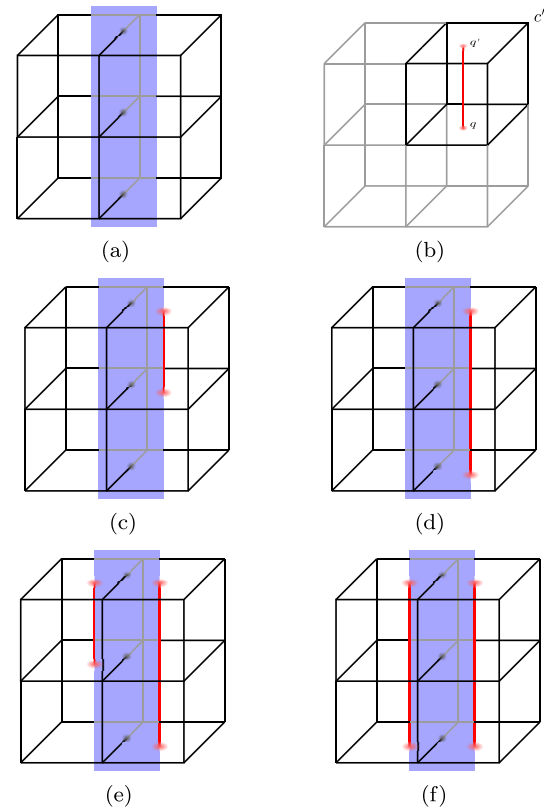

FIG. 8. In (a), we show an excited state of the toric code. In (b), we illustrate the graphical notation corresponding to add a cube operator $B_{c'}^{(z)}$ and remove the plaquette operators B_q and $B_{q'}$ of the toric code Hamiltonian. In (c), we take the model defined by the Hamiltonian obtained in figure (b) and consider the TC excited state of figure (a) in this context. It is still an excited state, but its energy is reduced by two unities. In (d), by continuously extending the red line of figure (c), we obtain a state with an even more reduced energy. In (e) and (f), the same procedure is done for all cubes hosting a half of the ribbon, resulting in a ground state.

z direction. The boundary of this ribbon is composed by two noncontractible curves. The energy of this state is two times the length L_z of the torus in the z direction.

We will now replace plaquette operators of the toric code with the cube operators defined in Eqs. (11)–(13). To better visualize what is happening, we assign the following graphical notation to the process of replacing plaquettes with cube operators: we draw a straight red line connecting two parallel plaquettes the operators of which are removed from the TC Hamiltonian. Then, to any cube hosting such a red line we associate a cube operator $B_c^{(\mu)}$, where μ is the direction parallel to the red line. As an example, in Fig. 8(b), we perform this procedure to the cube c', associating to it an $B_{c'}^{(z)}$ operator. In this example, the resulting Hamiltonian is

$$H'_{\mathrm{TC}} = -\sum_{v} A_v - \sum_{p \neq q,q'} B_p - B_{c'}^{(z)}.$$

Then, consider again the toric code excited state of Fig. 8(a), but now with a red line linking two parallel plaquettes in the z direction, as in Fig. 8(c). Now, the Hamiltonian of the model has a $B_c^{(z)}$ operator corresponding to the cube

hosting the red line. Since the plaquettes connected by the red line in the z direction share the same holonomy, the cube is not excited. Hence, the energy of the state is reduced by two unities. However, it is still an excited state of the toric code. The ground-state degeneracy of the toric code does not change under this modification of the Hamiltonian.

By continuously extending the red line of Fig. 8(c) to the boundary, we obtain Fig. 8(d). The red line closes into a noncontractible curve. The energy of the state is reduced to be equal to the length of the torus in the z direction. The resulting state of Fig. 8(d) is still an excited state of the toric code, and the corresponding modified Hamiltonian remains equivalent to H_{TC}.

The same procedure can be performed to the neighboring cubes that host the other half of the dual ribbon, as shown in Figs. 8(e) and 8(f). However, the resulting state in Fig. 8(f) is a ground state. Thus, the Hamiltonian obtained at the end of the process shown in Figs. 8(c)–8(f) defines a model in which ground states are given by closed dual surfaces and surfaces bounded by the red noncontractible curves. Its ground-state degeneracy is $\mathrm{GSD}_{\mathrm{TC}} + 2$, where $\mathrm{GSD}_{\mathrm{TC}}$ is the ground-state degeneracy of the toric code.

The procedure of connecting parallel plaquettes by red lines can be extended to the whole lattice at every direction. The resulting Hamiltonian is the one given by Eq. (14), and it describes the fractonlike model. In this way, there is a continuous process in which we can go from the toric code Hamiltonian to Eq. (14). In this process, TC excitations condense into ground states of the fractonlike model. However, note that only TC excitations given by noncontractible ribbons condense into fractonlike ground states. For instance, a TC excitation given by a contractible surface, as in Fig. 9(a), is a fracton excitation in the fractonlike model.

2. *Fracton excitations*

The elementary excited states $|\phi\rangle \in \mathcal{H}$ are such that either $A_v |\phi\rangle = 0$, for some vertex v, or $B_c^{(\mu)} |\phi\rangle = 0$, for some cube c and direction μ. A string of σ^z operators, beginning at a vertex v and ending at a vertex v', creates excitations of A_v and $A_{v'}$, also called charge excitations. Since A_v is essentially the gauge transformation of the 3D toric code, the charge excitations of the model (14) are the same charge excitations of the 3D toric code, and they can move freely in the lattice without an energy cost.

Now, excited states of the cube operators $B_c^{(\mu)}$ are called μ-flux excitations and can be pictured as lying at the corners of membranes. This can be better understood using the graphical representation of states as in Fig. 9. The simplest μ-flux excited state is created by the action of a σ^x operator on a single site over a ground state of the model. Note that whether this operator acts on a link along the x, y, or z axis will result in certain combinations of x, y, and z fluxes. For instance, acting with σ_l^x on a ground state,

$$|\phi\rangle = \sigma_l^x |\psi_0\rangle , \tag{20}$$

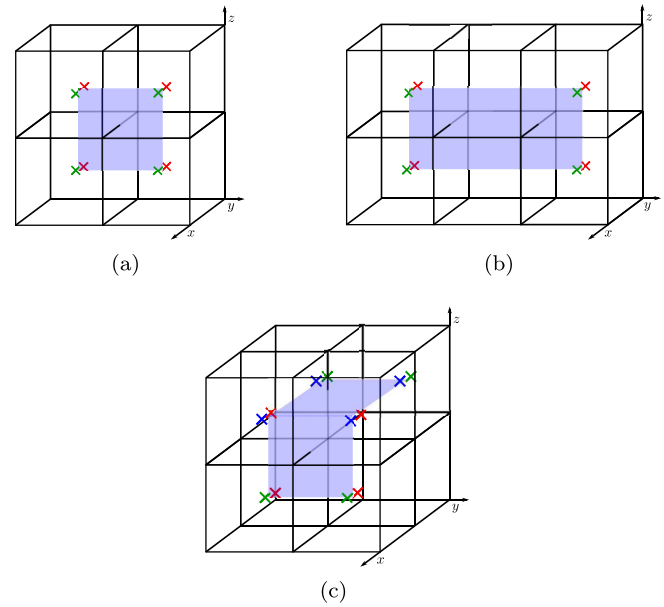

FIG. 9. (a) A state represented by the membrane diagram inside M has flux excitations and the four cubes at its corners. The red crosses represent what we call z fluxes, excitations of $B_c^{(z)}$, whereas the green ones are y fluxes, excitations of $B_c^{(y)}$. Blue crosses stand for x fluxes, excitations of $B_c^{(x)}$. (b) Excitations can freely move as long as the number of corners remains invariant. (c) If a membrane bends into an orthogonal direction, flux excitations are created at every corner it has.

where l is a x-like link, results in a state with pairs of y and z fluxes at the boundaries of the membrane as depicted in Fig. 9(a).

These excitations have restricted mobility since their localization is associated to the corners of the membrane. For example, the state represented by Fig. 9(b) shows that extending the membrane along the y direction moves pairs of μ fluxes. In general, moving these excitations corresponds to extending the membrane without changing the number of corners. In contrast, if the membrane is bent towards its orthogonal direction more excited states are created, increasing the energy of the state, as shown in Fig. 9(c). Again, this is interpreted as an energy penalization to deformations of membranes that change their number of corners.

IV. ENTANGLEMENT ENTROPY

In this section, we calculate the entanglement entropy S_A of a subregion A of the lattice for the models presented in Secs. II and III. For both cases, we interpret the result as a relation between the entanglement entropy of A and the ground-state degeneracy of a restriction of the full corresponding model to the subregion A.

A. Entanglement entropy of the 2D fractonlike model

Consider the 2D fractonlike model of Sec. II. The model is defined on a square lattice of size $L_x \times L_y$. Let us split the lattice into two subregions, A and B, as in Fig. 10, where subregion A is characterized by black vertices and has size

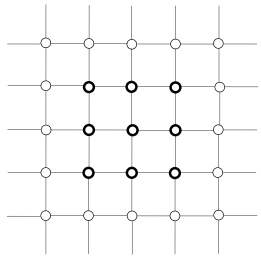

FIG. 10. Division of the lattice into two subregions, A and B, where region A is composed by black vertices.

$R_x \times R_y$. The total Hilbert space $\mathcal{H}$ is thus given by the tensor product $\mathcal{H} = \mathcal{H}_A \otimes \mathcal{H}_B$, where $\mathcal{H}_A$ and $\mathcal{H}_B$ are the Hilbert spaces associated to the regions A and B, respectively. We want to calculate the entanglement entropy S_A of subregion A. The density matrix of the model is given by

$$\rho = \frac{\Pi_0}{\mathrm{Tr}(\Pi_0)} = \frac{1}{\mathrm{GSD}}\Pi_0, \tag{21}$$

where GSD is the ground-state degeneracy given by Eq. (6) and Π_0 is the ground-state projector, given by

$$\Pi_0 = A\prod_p B_p, \tag{22}$$

where A is given by Eq. (3) and B_p by Eq. (2). The entanglement entropy is the *von Neumann entropy* of the reduced density matrix

$$S_A = -\mathrm{Tr}[\rho_A \log(\rho_A)], \tag{23}$$

where the reduced density matrix ρ_A is obtained from ρ by tracing out the region B, namely,

$$\rho_A = \mathrm{Tr}_B(\rho). \tag{24}$$

Taking the partial trace of ρ over region B, we have

$$\rho_A = \frac{1}{\mathrm{GSD}}\mathrm{Tr}_B\left[\frac{1}{2}\left(\bigotimes_{v\in K_0}\mathbb{1}_v + \bigotimes_{v\in K_0}\sigma_v^x\right)\prod_p B_p\right]. \tag{25}$$

The second term of the sum in the right-hand side of Eq. (25) multiplies a σ^x matrix to every vertex in the lattice. As we will see more clearly in what follows, the product $\prod_p B_p$ can be written as a sum over plaquettes of products of σ^z matrices. In this sum, there will be terms where there will be no σ^z matrix acting on the region B, and thus introducing a σ^x operator to this region and taking the trace over B will yield zero. For terms in the sum where there are σ^z matrices acting on vertices in the region B, the multiplication by σ^x results in $-i\sigma^y$, which also has trace zero. Therefore, the second term of the sum in the right-hand side of Eq. (25) is equal to zero, and we have

$$\rho_A = \frac{1}{2\mathrm{GSD}}\mathrm{Tr}_B\left(\prod_p B_p\right). \tag{26}$$

Now, using Eq. (2), we can expand the product $\prod_p B_p$ into the sum given by Eq. (27):

$$\prod_p B_p = \prod_p \frac{1}{2}\left(\bigotimes_{v\in p}\mathbb{1}_v + \bigotimes_{v\in p}\sigma_v^z\right) = \frac{1}{2^{N_p}}\left(\bigotimes_{v\in K_0}\mathbb{1}_v + \sum_p\bigotimes_{v\in p}\sigma_v^z + \sum_{p\neq q}\bigotimes_{v\in p}\sigma_v^z\bigotimes_{v'\in q}\sigma_{v'}^z + \ldots\right), \tag{27}$$

where N_p is the number of plaquettes in the lattice. To each plaquette, we assign an operator of the form $b_p = \bigotimes_{v\in p}\sigma_v^z$ and a number $s_p \in \{0, 1\}$. We also define the vector $s = (s_{p_1}, \ldots, s_{p_{N_p}})$, the ith entry of which is the number s_{p_i}, associated to the ith plaquette in the lattice. Then, for each possible vector s, we define the product

$$g_s = b_{p_1}^{s_{p_1}} b_{p_2}^{s_{p_2}} \ldots b_{p_{N_p}}^{s_{p_{N_p}}} \tag{28}$$

of operators b_p for every plaquette of the lattice. To illustrate, the vector $s_0 = (0, \ldots, 0)$ gives the product $g_{s_0} = \bigotimes_v \mathbb{1}_v$, while the vector $s_1 = (1, 0, \ldots, 0)$ gives the product $g_{s_1} = \bigotimes_{v\in p_1}\sigma_v^z$. It is straightforward to check that g_s, for every vector s, forms a finite Abelian group, which we call G. Also, the sum over all elements of G is equivalent to the sum in the expansion shown in Eq. (27). Therefore, since the trace will give zero whenever there are σ^z operators acting over the region B and the only surviving terms will be those with only identity operators acting over B, we can write

$$\begin{aligned}\rho_A &= \frac{1}{2^{N_p+1}\mathrm{GSD}}\mathrm{Tr}_B\left(\sum_{g_s\in G} g_s\right)\\ &= \frac{1}{2^{N_p+1}\mathrm{GSD}}\dim(\mathcal{H}_B)\sum_{g_s^A\in G} g_s^A,\end{aligned} \tag{29}$$

where g_s^A are the elements in G which have only identity operators acting over the subregion B, and they form a subgroup, which we call G^A. This implies that

$$\rho_A^2 = \frac{\dim(\mathcal{H}_B)}{2^{N_p+1}\mathrm{GSD}}|G^A|\rho_A, \tag{30}$$

where $|G^A|$ is the order of the subgroup G^A. Then, from Eqs. (23) and (30) it is easy to see that the entanglement entropy for subregion A is given by

$$S_A = \log\left(\frac{2^{N_p+1}\mathrm{GSD}}{|G^A|\dim(\mathcal{H}_B)}\right). \tag{31}$$

For a lattice with dimensions $L_x \times L_y$ and a subregion A with dimensions $R_x \times R_y$, with GSD given by Eq. (6), the entanglement entropy for the subregion A is

$$S_A = \log(2^{R_x+R_y+1}) = R_x + R_y + 1. \tag{32}$$

One can notice that there is a similarity between the functional dependence of the entanglement entropy (32) and the logarithm of the ground-state degeneracy of the same model defined only on the sublattice A. In fact, this result agrees with those in [62], where the entanglement entropy for some subregion A, for arbitrary topological models, was shown to

be equal to the logarithm of the ground-state degeneracy of the model restricted in a particular way to the subregion A, namely,

$$S_A = \log(\mathrm{GSD}_{\tilde{A}}), \tag{33}$$

where $\mathrm{GSD}_{\tilde{A}}$ is the ground state of the model restricted to subregion A and without the gauge transformations on the boundary of A. To see that this is indeed the case, let us calculate the ground-state degeneracy of the model given by Eq. (4) restricted to some subregion A of dimensions $R_x \times R_y$ and without gauge transformations on the boundary ∂A of A. Note that, since the transformations (3) act globally, the only way to exclude such transformations from the boundary ∂A is to exclude them from the whole lattice. Thus, the restricted model is given by

$$H_{\tilde{A}} = -\sum_{p\in A} B_p. \tag{34}$$

We can construct ground states of this model just like we did in Sec. II, but now every ground state we had will be split into two different ones. For example, the two states which form the superposition $|\psi_0\rangle$ of Fig. 2(a), which is a ground state of the full model, will be ground states of the restricted model (34). Thus, the model (34) has two times the degeneracy of the full model, and we have that

$$\mathrm{GSD}_{\tilde{A}} = 2^{R_x+R_y+1}. \tag{35}$$

We can immediately see that Eqs. (32) and (35) satisfy Eq. (33).

B. Entanglement entropy of the 3D fractonlike model

Now, consider the 3D fractonlike model of Sec. III, defined on a cubic lattice of size $L_x \times L_y \times L_z$. The calculation of the entanglement entropy for this model will follow almost exactly the previous one. We split the lattice into two subregions, A and B, where subregion A has dimensions $R_x \times R_y \times R_z$. The total Hilbert space $\mathcal{H}$ will then be given by the tensor product $\mathcal{H} = \mathcal{H}_A \otimes \mathcal{H}_B$ of the Hilbert spaces associated to subregions A and B. The density matrix is given by Eq. (21), where GSD is given by Eq. (17) and Π_0 will now be given by

$$\Pi_0 = \prod_v A_v \prod_{\mu,c} B_c^{(\mu)}, \tag{36}$$

where, for every vertex v, A_v is given by Eq. (10) and, for every cube c, $B_c^{(\mu)}$ is given by Eqs. (11), (12), and (13), for $\mu = x, y, z$ respectively. From the definitions of the cube operators, it follows that for a fixed cube c

$$B_c^{(x)} B_c^{(y)} B_c^{(z)} = \tfrac{1}{4}\left(\mathbb{1} + Z_c^{(x)} + Z_c^{(y)} + Z_c^{(z)}\right), \tag{37}$$

where

$$Z_c^{(x)} \left| \quad \right\rangle = \left| \quad \right\rangle, \tag{38}$$

$$Z_c^{(y)} \left| \quad \right\rangle = \left| \quad \right\rangle, \tag{39}$$

$$Z_c^{(z)} \left| \quad \right\rangle = \left| \quad \right\rangle. \tag{40}$$

Then, we have

$$\Pi_0 = \frac{1}{2^{N_v+2N_c}} \prod_v (\mathbb{1}_v + X_v) \prod_c \left(\mathbb{1}_c + \sum_\mu Z_c^{(\mu)}\right), \tag{41}$$

where $\mathbb{1}_v = \bigotimes_{l\in \mathrm{star}(v)} \mathbb{1}_l$, $X_v = \bigotimes_{l\in \mathrm{star}(v)} \sigma_l^x$, $\mu = x, y, z$, N_v is the number of vertices, and N_c is the number of cubes in the lattice. This product is equal to a sum of products of Pauli matrices, and thus we can proceed just as we did in the case of the 2D model by defining a group G the elements g_s of which, indexed by a vector s with $N_v + 2N_c$ components, with each component being zero or one, are given by products of Pauli matrices, in a similar way as in Eq. (28). The result is that

$$\Pi_0 = \frac{1}{2^{N_v+2N_c}} \sum_{g_s\in G} g_s. \tag{42}$$

From Eq. (24), the reduced density matrix ρ_A is then given by

$$\rho_A = \frac{1}{2^{N_v+2N_c}} \dim(\mathcal{H}_B) \sum_{g_s^{\tilde{A}}\in G} g_s^{\tilde{A}}, \tag{43}$$

where $\tilde{A}$ is a region obtained from A by excluding the vertices at the boundary ∂A of A. The reason this is the only surviving region after we take the trace over B is that gauge transformations A_v that act over vertices v on the boundary of A can introduce σ^x operators acting over links outside of A, i.e., links that belong to B. The trace over B then gives zero in such case.

It is straightforward to check that the elements $g_s^{\tilde{A}}$ form a subgroup of G. Thus, we can perform exactly the same steps we did in Sec. IV A and then, using Eq. (23), it follows that the entanglement entropy of subregion A is given by

$$S_A = \log\left(\frac{2^{N_v+2N_c}\mathrm{GSD}}{|G^{\tilde{A}}|\dim(\mathcal{H}_B)}\right), \tag{44}$$

where $|G^{\tilde{A}}|$ is the order of the subgroup $G^{\tilde{A}}$ formed by the elements $g_s^{\tilde{A}}$. Since the lattice has dimension $L_x \times L_y \times L_z$ and region A has dimension $R_x \times R_y \times R_z$, we have that

$$S_A = 3(R_xR_y + R_xR_z + R_yR_z) + 2, \tag{45}$$

and this result is also consistent with Eq. (33). To see this, let us calculate the ground state $\mathrm{GSD}_{\tilde{A}}$ of the reduced model. To reduce the model, we must discard the gauge transformations on the boundary of region A. This means that configurations which differ from each other only by a gauge transformation

on the boundary ∂A are not gauge equivalent anymore, and must be accounted for in the calculation of $\mathrm{GSD}_{\tilde{A}}$. So, the number of configurations to be added to GSD is the number of gauge transformations on the boundary ∂A, which is simply the number of vertices in ∂A, and this number is equal to $2(R_xR_y + R_xR_z + R_yR_z) + 2$. Thus, $\mathrm{GSD}_{\tilde{A}} = R_xR_y + R_xR_z + R_yR_z + 2(R_xR_y + R_xR_z + R_yR_z) + 2$ and Eq. (33) holds.

The constant term in Eq. (45) is equal to the topological entanglement entropy of the 3D toric code. This is expected because, as we discussed in Sec. III B 1, toric code ground states belong to the set of ground states of the fractonlike model.

V. REMARKS ON GENERALIZATIONS TO ARBITRARY GAUGE GROUPS

The models presented in Secs. II and III can be generalized to models based on arbitrary, possibly non-Abelian finite groups. In this section, we make some remarks about how this generalization could be done. We leave a more in-depth discussion for future work.

A. *G* fractonlike order in two dimensions

Consider a two-dimensional oriented manifold M, discretized by a square lattice. At each vertex v, we have a local Hilbert space $\mathcal{H}_v$ with basis given by states $|g\rangle$ labeled by some element $g \in G$, where G is an arbitrary finite group and the total Hilbert space is $\mathcal{H} = \bigotimes_v \mathcal{H}_v$. Global gauge transformations are given by

$$A^g|a, b, c, ...\rangle = |ga, gb, gc, ...\rangle\,, \tag{46}$$

where $g \in G$ and $|a, b, c, ...\rangle \in \mathcal{H}$ is an arbitrary basis state in the total Hilbert space, with $a, b, c, ... \in G$. We define the operator A as the normalized sum of all global gauge transformations, namely,

$$A = \frac{1}{|G|}\sum_{g\in G} A^g. \tag{47}$$

One can easily see that if $G = \mathbb{Z}_2$ we recover Eq. (3). Next, we define two plaquette operators $B_p^{(\mu)}$, $\mu = x, y$, which in the language of higher gauge theories (see [22]) act by comparing the zero holonomy of links that are parallel to the μ direction. They are given by the formulas

$B_p^{(x)}$ 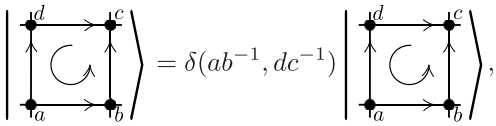 $= \delta(ab^{-1}, dc^{-1})$, (48)

$B_p^{(y)}$ 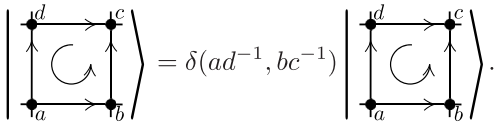 $= \delta(ad^{-1}, bc^{-1})$. (49)

If G is Abelian, the two operators are actually the same, and one can easily check that if $G = \mathbb{Z}_2$ we recover Eq. (2). The Hamiltonian is then given by

$$H = -A - \sum_p \left(B_p^{(x)} + B_p^{(y)}\right). \tag{50}$$

One may notice a similarity between this theory and the usual quantum double model of the finite group G [5,7–9]. In fact, the operators defined in (46), (48), and (49) satisfy the quantum double algebra $D(G)$. Define the local operators $L_v^g, R_v^g, T_v^g : \mathcal{H}_v \to \mathcal{H}_v$ such that $\forall\, |a\rangle \in \mathcal{H}_v$:

$$L_v^g\,|a\rangle = |ga\rangle\,, \tag{51}$$

$$R_v^g\,|a\rangle = |ag\rangle\,, \tag{52}$$

$$T_v^g\,|a\rangle = \delta(g, a)\,|a\rangle\,. \tag{53}$$

These operators satisfy the quantum double algebra $D(G)$ [5]. We can write A and $B_p^{(\mu)}$, for every p, in terms of L_v^g, R_v^g, and T_v^g in the following way. First, from (46), we have that

$$A^g = \bigotimes_v L_v^g. \tag{54}$$

Now, for every plaquette $p = (v_1v_2v_3v_4)$, we define the operators

$$B_p^{(x)}(g) = \sum_{\{b_i\}_{i=1}^4} \delta\left(b_1b_2^{-1}b_3b_4^{-1}, g\right) \bigotimes_{v_i\in p} T_{v_i}^{b_i}, \tag{55}$$

$$B_p^{(y)}(g) = \sum_{\{b_i\}_{i=1}^4} \delta\left(b_1b_4^{-1}b_3b_2^{-1}, g\right) \bigotimes_{v_i\in p} T_{v_i}^{b_i}. \tag{56}$$

For $g = e$, the group identity, $B_p^{(x)}(e) = B_p^{(x)}$ and $B_p^{(y)}(e) = B_p^{(y)}$, where $B_p^{(x)}$ and $B_p^{(y)}$ are defined in (48) and (49), respectively. With these definitions, it is straightforward to check that the operators A and B_p do indeed satisfy the quantum double algebra of G, i.e., $\forall g, h \in G$:

$$A^gA^h = A^{gh}, \tag{57}$$

$$A^gB_p^{(\mu)}(h) = B_p^{(\mu)}(ghg^{-1})A^g, \tag{58}$$

for any $\mu = x, y$.

The algebra of the operators (47)–(49) is the quantum double of G, but the model (50) is different from the usual quantum double models. Here, we have a quantum double algebra for each plaquette in the lattice, while in the usual QDMs there is an algebra for each vertex-plaquette pair. A consequence of this fact is that there are no dyons here, only flux quasiparticles. However, the fact that the operator algebra in this model is the quantum double of G allows us to immediately classify the flux quasiparticles of the model. A more in-depth discussion about this topic will appear in a future work.

B. *G* fractonlike order in three dimensions

Consider a three-dimensional oriented manifold M, discretized by a regular cubic lattice. At each link l, there is a local Hilbert space $\mathcal{H}_l$, generated by a set $\{|g\rangle\}$ of basis elements, labeled by some finite group G. The total Hilbert

space is given by the product $\mathcal{H} = \bigotimes_l \mathcal{H}_l$. We define three cube operators $B_c^{(\mu)}$, one for each direction $\mu = x, y, z$. $B_c^{(\mu)}$ compares the one holonomy of plaquettes that are orthogonal to the μ direction, in the following way:

$$B_c^{(x)} \left| \begin{array}{c} \\ \\ \\ \\ \\ \\ \\ \\ \end{array} \right\rangle = \delta(a_1 c_1 b_1^{-1} c_4^{-1}, a_3 c_2 b_3^{-1} c_3^{-1}) \left| \begin{array}{c} \\ \\ \\ \\ \\ \\ \\ \\ \end{array} \right\rangle, \tag{59}$$

$$B_c^{(y)} \left| \begin{array}{c} \\ \\ \\ \\ \\ \\ \\ \\ \end{array} \right\rangle = \delta(a_2 c_2 b_2^{-1} c_1^{-1}, a_4 c_4 b_4^{-1} c_4^{-1}) \left| \begin{array}{c} \\ \\ \\ \\ \\ \\ \\ \\ \end{array} \right\rangle, \tag{60}$$

$$B_c^{(z)} \left| \begin{array}{c} \\ \\ \\ \\ \\ \\ \\ \\ \end{array} \right\rangle = \delta(a_1 a_2 a_3^{-1} a_4^{-1}, b_1 b_2 b_3^{-1} b_4^{-1}) \left| \begin{array}{c} \\ \\ \\ \\ \\ \\ \\ \\ \end{array} \right\rangle. \tag{61}$$

It turns out that, for arbitrary groups, it is not possible to define an operator analogous to (10) which commutes with every cube operator. However, we can define a global operator A, inspired by the 2D model of Sec. V A, made of a suitable combination of L^g's and R^g's to make it commute with all the cube operators. Then, we define a global operator

$$A = \frac{1}{|G|} \sum_{g \in G} A^g, \tag{62}$$

where A^g is defined as

$$A^g = \bigotimes_p L^g_{l_1} \otimes R^g_{l_2} \otimes R^g_{l_3} \otimes L^g_{l_4}, \tag{63}$$

where $l_i \in \partial p$, $i = 1, ..., 4$ and the plaquettes are oriented outwards.

The Hamiltonian is defined as

$$H = -A - \sum_c \left(B_c^{(x)} + B_c^{(y)} + B_c^{(z)} \right). \tag{64}$$

The operators defined in Eqs. (62), (59), (60), and (61) commute for every cube in the lattice, so the Hamiltonian (64) can be diagonalized. Moreover, as in Sec. V A, we can write these operators in terms of L^g's, R^g's, and T^g, and then it can be shown that they also satisfy the quantum double algebra of G. We leave this discussion for a future work.

VI. CONCLUSIONS AND OUTLOOK

In this paper, we have studied models of fractonlike order based on lattice gauge theory with subsystem symmetries in two and three spatial dimensions. The three-dimensional model reduces to the 3D toric code when subsystem symmetry is explicitly broken, realizing an example of a subsystem-symmetry enriched topological phase. It exhibits some features that are usually not present in the most common realizations of fracton order, such as a ground-state degeneracy that depends exponentially on square of the linear size of the system and on its topology, and fully mobile excitations living along with fractons. However, the fractonlike character is destroyed if local perturbations that break the subsystem symmetry are applied to the system. We also calculated the entanglement entropy of these models, and we showed that it obeys a simple formula which was derived for the case of usual topological models, relating the entanglement entropy and the ground-state degeneracy of a particularly restricted model. Although they are not topologically protected, these models show that one can obtain fractonlike phases from more regular lattice gauge theories, giving an alternative to the usual constructions found in the literature.

One important open question is how the models introduced in this paper and more standard models such as the X-cube model are connected. Since the ground-state degeneracy of the model described in Sec. III scales differently from the X cube, a relation between the two is not obvious. Likewise, it is not clear what is the relation between the generalized lattice gauge theory with subsystem symmetries of [24,55,56] and the approach developed in this paper.

Moreover, the definitions of the models in Secs. II, III, and V show an explicit dependence on the geometry and the topology of the system, which suggests that new phenomena may arise if we define the models in manifolds with nontrivial geometry, topology, and discretization. This direction was pursued for the X-cube model [71,72], and therefore it may

also be helpful in the quest to clarify how the two models are connected.

At the end of this paper we made some remarks about the possibility of constructing fractonlike models from non-Abelian gauge groups. We argued that the operator algebra of these models is the quantum double of the corresponding finite group, but the models constructed in this way are not equivalent to the known quantum double models. This direction is worth pursuing because this construction allows us to study more directly the behavior of non-Abelian fractons, which are known in the literature [57,73]. This could possibly lead to a better understanding of how to apply fracton phases in quantum computation. On the other hand, the entanglement entropy can certainly give more information about the nature of entanglement in the ground/excited states of the fracton models we introduce in this paper. In [62], we show that the entanglement entropy calculation can be mapped into the counting of edge states in the entanglement cut. This also holds for the fractonlike models of this paper, and whether it is also the case for more standard fracton models is an immediate question worthy of further study that could deepen our understanding of gapped quantum phases of matter.

ACKNOWLEDGMENTS

We thank Kevin Slagle, Dominic J. Williamson, and Abhinav Prem for useful comments and suggestions. J.P.I.J. thanks CNPq (Grant No. 162774/2015-0) for support during this work. L.N.Q.X. thanks CNPq (Grant No. 164523/2018-9) for supporting this work. M.P. is supported by CAPES.

[1] D. C. Tsui, H. L. Stormer, and A. C. Gossard, Two-Dimensional Magnetotransport in the Extreme Quantum Limit, Phys. Rev. Lett. **48**, 1559 (1982).

[2] R. B. Laughlin, Anomalous Quantum Hall Effect: An Incompressible Quantum Fluid with Fractionally Charged Excitations, Phys. Rev. Lett. **50**, 1395 (1983).

[3] X. G. Wen and Q. Niu, Ground-state degeneracy of the fractional quantum Hall states in the presence of a random potential and on high-genus Riemann surfaces, Phys. Rev. B **41**, 9377 (1990).

[4] X. Chen, Z. C. Gu, and X. G. Wen, Local unitary transformation, long-range quantum entanglement, wave function renormalization, and topological order, Phys. Rev. B **82**, 155138 (2010).

[5] A. Yu. Kitaev, Fault-tolerant quantum computation by anyons, Ann. Phys. (NY) **303**, 2 (2003).

[6] C. Nayak, S. H. Simon, A. Stern, M. Freedman, and S. D. Sarma, Non-Abelian anyons and topological quantum computation, Rev. Mod. Phys. **80**, 1083 (2008).

[7] H. Bombin and M. A. Martin-Delgado, Family of non-Abelian Kitaev models on a lattice: Topological condensation and confinement, Phys. Rev. B **78**, 115421 (2008).

[8] O. Buerschaper and M. Aguado, Mapping Kitaev's quantum double lattice models to Levin and Wen's string-net models, Phys. Rev. B **80**, 155136 (2009).

[9] M. J. B. Ferreira, P. Padmanabhan, and P. Teotonio-Sobrinho, 2D quantum double models from a 3D perspective, J. Phys. A: Math. Theor. **47**, 375204 (2014).

[10] X. Chen, Z. C. Gu, Z. X. Liu, and X. G. Wen, Symmetry protected topological orders and the group cohomology of their symmetry group, Phys. Rev. B **87**, 155114 (2013).

[11] A. Kapustin, Symmetry protected topological phases, anomalies, and cobordisms: Beyond group cohomology, arXiv:1403.1467.

[12] A. Mesaros and Y. Ran, Classification of symmetry enriched topological phases with exactly solvable models, Phys. Rev. B **87**, 155115 (2013).

[13] Y. M. Lu and A. Vishwanath, Classification and properties of symmetry-enriched topological phases: Chern-Simons approach with applications to Z_2 spin liquids, Phys. Rev. B **93**, 155121 (2016).

[14] M. Barkeshli, P. Bonderson, M. Cheng, and Z. Wang, Symmetry fractionalization, defects, and gauging of topological phases, Phys. Rev. B **100**, 115147 (2019).

[15] M. Cheng, Z. C. Gu, S. Jiang, and Y. Qi, Exactly solvable models for symmetry-enriched topological phases, Phys. Rev. B **96**, 115107 (2017).

[16] V. G. Turaev and A. Virelizier, *Monoidal Categories and Topological Field Theory*, Progress in Mathematics Vol. 322 (Springer, New York, 2017).

[17] M. A. Levin and X. G. Wen, String-net condensation: A physical mechanism for topological phases, Phys. Rev. B **71**, 045110 (2005).

[18] J. C. Baez and U. Schreiber, Higher gauge theory, arXiv:math/0511710.

[19] J. C. Baez and J. Huerta, An invitation to higher gauge theory, Gen. Rel. Grav. **43**, 2335 (2011).

[20] A. Bullivant, M. Calçada, Z. Kádár, P. Martin, and J. F. Martins, Topological phases from higher gauge symmetry in 3 + 1 dimensions, Phys. Rev. B **95**, 155118 (2017).

[21] C. Delcamp and A. Tiwari, From gauge to higher gauge models of topological phases, J. High Energy Phys. 10 (2018) 049.

[22] R. C. de Almeida, J. P. Ibieta-Jimenez, J. L. Espiro, and P. Teotonio-Sobrinho, Topological order from a cohomological and higher gauge theory perspective, arXiv:1711.04186.

[23] C. Chamon, Quantum Glassiness in Strongly Correlated Clean Systems: An Example of Topological Overprotection, Phys. Rev. Lett. **94**, 040402 (2005).

[24] S. Vijay, J. Haah, and L. Fu, Fracton topological order, generalized lattice gauge theory, and duality, Phys. Rev. B **94**, 235157 (2016).

[25] R. M. Nandkishore and M. Hermele, Fractons, Ann. Rev. Condens. Matter Phys. **10**, 295 (2019).

[26] A. Dua, I. H. Kim, M. Cheng, and D. J. Williamson, Sorting topological stabilizer models in three dimensions, Phys. Rev. B **100**, 155137 (2019).

[27] Z. Weinstein, E. Cobanera, G. Ortiz, and Z. Nussinov, Absence of finite temperature phase transitions in the X-cube model and its Z_p generalization, Ann. Phys. (NY) **412**, 168018 (2020).

[28] J. Haah, Local stabilizer codes in three dimensions without string logical operators, Phys. Rev. A **83**, 042330 (2011).

[29] C. Castelnovo, C. Chamon, and D. Sherrington, Quantum mechanical and information theoretic view on classical glass transitions, Phys. Rev. B **81**, 184303 (2010).
[30] C. Castelnovo and C. Chamon, Topological quantum glassiness, Philos. Mag. **92**, 304 (2012).
[31] I. H. Kim and J. Haah, Localization from Superselection Rules in Translationally Invariant Systems, Phys. Rev. Lett. **116**, 027202 (2016).
[32] A. Prem, J. Haah, and R. Nandkishore, Glassy quantum dynamics in translation invariant fracton models, Phys. Rev. B **95**, 155133 (2017).
[33] S. Pai, M. Pretko, and R. M. Nandkishore, Localization in Fractonic Random Circuits, Phys. Rev. X **9**, 021003 (2019).
[34] S. Bravyi and J. Haah, Energy Landscape of 3D Spin Hamiltonians with Topological Order, Phys. Rev. Lett. **107**, 150504 (2011).
[35] S. Bravyi, B. Leemhuis, and B. M. Terhal, Topological order in an exactly solvable 3D spin model, Ann. Phys. (NY) **326**, 839 (2011).
[36] I. H. Kim, 3D local qupit quantum code without string logical operator, arXiv:1202.0052.
[37] S. Bravyi and J. Haah, Quantum Self-Correction in the 3D Cubic Code Model, Phys. Rev. Lett. **111**, 200501 (2013).
[38] R. Raussendorf, C. Okay, D. S. Wang, D. T. Stephen, and H. P. Nautrup, Computationally Universal Phase of Quantum Matter, Phys. Rev. Lett. **122**, 090501 (2019).
[39] T. Devakul and D. J. Williamson, Universal quantum computation using fractal symmetry-protected cluster phases, Phys. Rev. A **98**, 022332 (2018).
[40] D. T. Stephen, H. P. Nautrup, J. Bermejo-Vega, J. Eisert, and R. Raussendorf, Subsystem symmetries, quantum cellular automata, and computational phases of quantum matter, Quantum **3**, 142 (2019).
[41] M. Pretko, Subdimensional particle structure of higher rank $U(1)$ spin liquids, Phys. Rev. B **95**, 115139 (2017).
[42] M. Pretko, Generalized electromagnetism of subdimensional particles: A spin liquid story, Phys. Rev. B **96**, 035119 (2017).
[43] K. Slagle, A. Prem, and M. Pretko, Symmetric tensor gauge theories on curved spaces, Ann. Phys. (NY) **410**, 167910 (2019).
[44] D. Bulmash and M. Barkeshli, Higgs mechanism in higher-rank symmetric U(1) gauge theories, Phys. Rev. B **97**, 235112 (2018).
[45] H. Ma, E. Lake, X. Chen, and M. Hermele, Fracton topological order via coupled layers, Phys. Rev. B **95**, 245126 (2017).
[46] M. Pretko, The fracton gauge principle, Phys. Rev. B **98**, 115134 (2018).
[47] M. Pretko, Emergent gravity of fractons: Mach's principle revisited, Phys. Rev. D **96**, 024051 (2017).
[48] M. Pretko and L. Radzihovsky, Fracton-Elasticity Duality, Phys. Rev. Lett. **120**, 195301 (2018).
[49] A. Gromov, Chiral Topological Elasticity and Fracton Order, Phys. Rev. Lett. **122**, 076403 (2019).
[50] H. Ma, M. Hermele, and X. Chen, Fracton topological order from the Higgs and partial-confinement mechanisms of rank-two gauge theory, Phys. Rev. B **98**, 035111 (2018).
[51] H. Yan, Hyperbolic fracton model, subsystem symmetry, and holography, Phys. Rev. B **99**, 155126 (2019).
[52] H. Yan, Hyperbolic fracton model, subsystem symmetry, and holography. II. The dual eight-vertex model, Phys. Rev. B **100**, 245138 (2019).
[53] S. Vijay, Isotropic layer construction and phase diagram for fracton topological phases, arXiv:1701.00762.
[54] K. Slagle, D. Aasen, and D. Williamson, Foliated field theory and string-membrane-net condensation picture of fracton order, SciPost Phys. **6**, 043 (2019).
[55] W. Shirley, K. Slagle, and X. Chen, Foliated fracton order from gauging subsystem symmetries, SciPost Phys. **6**, 041 (2019).
[56] D. J. Williamson, Fractal symmetries: Ungauging the cubic code, Phys. Rev. B **94**, 155128 (2016).
[57] H. Song, A. Prem, S. J. Huang, and M. A. Martin-Delgado, Twisted fracton models in three dimensions, Phys. Rev. B **99**, 155118 (2019).
[58] D. J. Williamson, Z. Bi, and M. Cheng, Fractonic matter in symmetry-enriched $U(1)$ gauge theory, Phys. Rev. B **100**, 125150 (2019).
[59] O. Petrova and N. Regnault, Simple anisotropic three-dimensional quantum spin liquid with fractonlike topological order, Phys. Rev. B **96**, 224429 (2017).
[60] D. Bulmash and M. Barkeshli, Gauging fractons: Immobile non-Abelian quasiparticles, fractals, and position-dependent degeneracies, Phys. Rev. B **100**, 155146 (2019).
[61] A. Prem and D. J. Williamson, Gauging permutation symmetries as a route to non-Abelian fractons, SciPost Phys. **7**, 68 (2019).
[62] J. P. Ibieta-Jimenez, M. Petrucci, L. N. Xavier, and P. Teotonio-Sobrinho, Topological entanglement entropy in d-dimensions for Abelian higher gauge theories, J. High Energ. Phys. 03 (2020) 167.
[63] C. Xu and J. E. Moore, Strong-Weak Coupling Self-Duality in the Two-Dimensional Quantum Phase Transition Of $p + ip$ Superconducting Arrays, Phys. Rev. Lett. **93**, 047003 (2004).
[64] C. Xu and J. E. Moore, Reduction of effective dimensionality in lattice models of superconducting arrays and frustrated magnets, Nucl. Phys. B **716**, 487 (2005).
[65] Y. You, T. Devakul, F. J. Burnell, and S. L. Sondhi, Subsystem symmetry protected topological order, Phys. Rev. B **98**, 035112 (2018).
[66] R. J. Baxter, *Exactly Solved Models in Statistical Mechanics* (Elsevier, Amsterdam, 2016).
[67] G. K. Savvidy and F. J. Wegner, Geometrical string and spin systems, Nucl. Phys. B **413**, 605 (1994).
[68] G. K. Savvidy, The system with exponentially degenerate vacuum state, arXiv:cond-mat/0003220.
[69] D. Espriu and A. Prats, Dynamics of the two-dimensional gonihedric spin model, Phys. Rev. E **70**, 046117 (2004).
[70] D. Espriu and A. Prats, On gonihedric loops and quantum gravity, J. Phys. A: Math. Gen. **39**, 1743 (2006).
[71] K. Slagle and Y. B. Kim, X-cube model on generic lattices: Fracton phases and geometric order, Phys. Rev. B **97**, 165106 (2018).
[72] W. Shirley, K. Slagle, Z. Wang, and X. Chen, Fracton Models on General Three-Dimensional Manifolds, Phys. Rev. X **8**, 031051 (2018).
[73] A. Prem, S. J. Huang, H. Song, and M. Hermele, Cage-Net Fracton Models, Phys. Rev. X **9**, 021010 (2019).